Mizokawa. *Microstructures* **2025**, *5*, 2025026
DOI: 10.20517/microstructures.2024.99

Microstructures

Research Article

Open Access

Check for updates

Charge/orbital disordered states with smaller volume and higher entropy in transition-metal oxides

Takashi Mizokawa

Department of Applied Physics, Waseda University, Tokyo 169-8555, Japan.

Correspondence to: Dr. Takashi Mizokawa, Department of Applied Physics, Waseda University, 3-4-1 Okubo, Shinjuku, Tokyo 169-8555, Japan. E-mail: mizokawa@waseda.jp

How to cite this article: Mizokawa, T. Charge/orbital disordered states with smaller volume and higher entropy in transition-metal oxides. *Microstructures* **2025**, *5*, 2025026. https://dx.doi.org/10.20517/microstructures.2024.99

Received: 15 Oct 2024 **First Decision:** 16 Dec 2024 **Revised:** 23 Dec 2024 **Accepted:** 3 Jan 2024 **Published:** 14 Mar 2025

Academic Editor: Andrea Sanson **Copy Editor:** Fangling Lan **Production Editor:** Fangling Lan

Abstract

Some transition-metal oxides such as Ca_2RuO_4, $BiNiO_3$, and V_2OPO_4 harbor smaller volume and higher entropy states by role sharing of the spin, charge, and orbital degrees of freedom. Effect of lattice distortions on the various charge/orbital patterns can be analyzed by *d*-*p* models with full degeneracy of the transition-metal *d* and oxygen 2*p* orbitals. Based on the mean-field analyses on the *d*-*p* models for Ca_2RuO_4, $BiNiO_3$ and V_2OPO_4, possible mechanisms of negative thermal expansion with charge and orbital degrees of freedom are discussed. In Ca_2RuO_4 and $BiNiO_3$, orbital and/or charge states are rearranged across their insulator-metal transitions, and the metallic phases with orbital and/or charge fluctuations can be stabilized at high temperatures relative to the insulating phases without them. In V_2OPO_4, the charge/orbital disordered state can keep relatively smaller volume due to orbital-dependent hybridization in the face-sharing VO_6 octahedron chain.

Keywords: Transition-metal oxides, charge order, orbital order, spin-orbit interaction, charge disproportionation, oxygen hole

INTRODUCTION

Transition-metal oxides exhibit surprisingly rich electrical, magnetic, and structural properties due to the correlated d electrons[1,2]. The d orbitals with five-fold degeneracy in the atomic limit are split into three-fold degenerate t_{2g} (*xy*, *yz*, and *zx*) and two-fold degenerate e_g ($3z^2$-r^2 and x^2-y^2) orbitals under the cubic ligand field. When the number of d electrons per transition-metal site is integer, the d electrons can be localized with the strong on-site electron-electron interaction (Mott insulators). A typical phase diagram of such Mott insulators is illustrated in Figure 1A. For example, pyrite-type NiS_2 exhibits a pressure-induced phase transition from a Mott insulator to a paramagnetic metal[1,2]. The paramagnetic metallic phase with itinerant d electrons has smaller volume than the Mott insulating phase with localized d electrons. In the Mott insulating phase, the localized spins tend to order antiferromagnetically (sometimes ferromagnetically) unless strong frustration effect sets in due to lattice geometry or other degrees of freedom. In NiS_2 with a face-centered cubic lattice, the Ni^{2+} ion (d^8 configuration with $S = 1$) does not have orbital degrees of freedom, and the $S = 1$ spins are antiferromagnetically ordered at low temperatures. In the paramagnetic insulating phase, the disordered spins can provide entropy of $k_B$log3 per Ni site. Since the symmetry of the paramagnetic insulating phase is the same as that of the paramagnetic metallic phase, their phase boundary is terminated at the critical point. In such a case without orbital degrees of freedom, the paramagnetic insulating phase with relatively large volume is stabilized at high temperatures due to the spin entropy $k_B$log3 per Ni relative to the paramagnetic metallic phase without it. Therefore, it is rather difficult to realize negative thermal expansion (NTE). On the other hand, in Mott insulators with orbital degrees of freedom, magnetic ordering temperature is usually lower than the orbital ordering temperature[1,2]. This suggests that the paramagnetic insulating phase can be accompanied by orbital order which is driven by electron-electron and/or electron-lattice interaction. If the orbital order survives up to the insulator-metal transition temperature, the symmetry of the paramagnetic insulating phase differs from that of the paramagnetic metallic phase which can be stabilized at high temperatures [Figure 1B]. A layered perovskite Ca_2RuO_4 is one of such examples in which orbital degrees of freedom play a vital role at the insulator-metal transition[3], and, indeed NTE in the temperature range 150-700 K was reported in Sn-doped Ca_2RuO_4 by Takenaka *et al.*[4]. When the charge-transfer energy between the transition-metal d orbitals and the oxygen 2p orbitals becomes close to zero or negative, charge degrees of freedom may play significant roles. Perovskite-type $RNiO_3$ (R = rare earth) indeed has almost zero or negative charge-transfer energy and the metal-insulator transition is assigned to $2Ni^{3+}(d^8L) \rightarrow Ni^{2+}(d^8) + Ni^{4+}(d^8L^2)$ charge disproportionation rather than Mott localization[5]. Here, L represents a hole in the O 2p orbitals. In the case of $BiNiO_3$, the oxygen 2p hole is bound to the Bi site, and, consequently, the valence state of $Bi^{3+}_{0.5}Bi^{5+}_{0.5}Ni^{2+}O_3$ is realized[6]. The electronic configuration of Bi^{5+} is s^2L^2 rather than s^0. Such oxygen 2*p* charge degrees of freedom are involved in the insulator-to-metal transition of $BiNiO_3$ and its sister materials. The high-temperature metallic phase with $Bi^{3+}Ni^{3+}O_3$ has smaller volume than the insulating phase of $Bi^{3+}_{0.5}Bi^{5+}_{0.5}Ni^{2+}O_3$, providing the NTE in La-doped $BiNiO_3$ with a temperature range of 320-380 K as discovered by Azuma *et al.*[6]. More recently, Pachoud *et al.* have discovered NTE behaviors with the temperature range of 600-700 K in V_2OPO_4 where both the charge and orbital degrees freedom are important[7]. The V^{2+}/V^{3+} mixed valence and V 3d orbital polarization have been observed by x-ray absorption/photoemission spectroscopy[8,9]. It has been established that the Bi-Ni charge transfer and the V-V charge transfer are responsible for the NTE of $BiNiO_3$[6] and V_2OPO_4[7].

When the charge/orbital orderings are associated with magnetic ordering and electron-electron interaction, the charge/orbital ordered states at low temperatures tend to have relatively large volume due to the localized d electrons with weak hybridization between neighboring d electrons. When the charge/orbital ordering is driven by formation of spin singlet bonds due to electron-lattice interaction (such as $CuIr_2S_4$ and $MgTi_2O_4$), the charge/orbital ordered state at low temperature has smaller volume. In the former case, since the exchange interaction between localized spins depends on the charge and orbital arrangement, the magnetic ordering temperature is usually lower than the charge and/or orbital ordering temperature. There are several types of lattice distortions to stabilize their charge/orbital order: Jahn-Teller distortion for Ca_2RuO_4/V_2OPO_4 and breathing distortion for $BiNiO_3$. The lattice distortions are removed in the

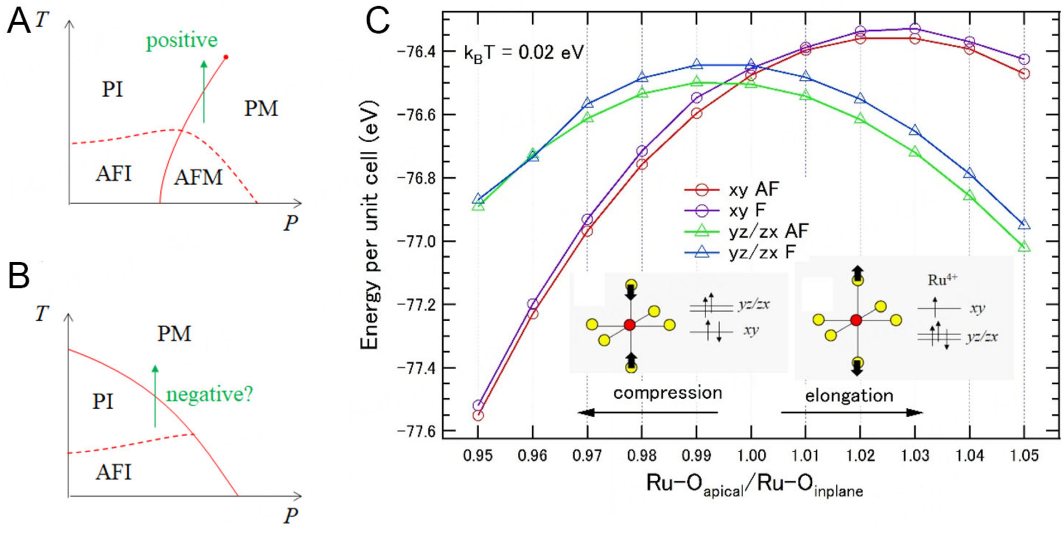

Figure 1. (A) Schematic phase diagram of NiS_2 as functions of temperature *T* and pressure *P*. (B) Schematic phase diagram of Ca_2RuO_4. PI, AFI, PM, and AFM represent paramagnetic insulating, antiferromagnetic insulating, paramagnetic metallic, and antiferromagnetic metallic phases. (C) Energy per unit cell calculated by mean-filed approximation for the layered perovskite-type *d-p* model with d^4 as a function of Jahn-Teller distortion (the ratio between the compressed/elongated apical Ru-O bond length and the in-plane Ru-O bond length. F and AF represent ferromagnetic and antiferromagnetic states. With the compression (elongation), the *xy* (*yz* or *zx*) orbitals are doubly occupied.

paramagnetic metallic phase with smaller volume, and the additional entropy by charge/orbital fluctuations helps the NTE of Ca_2RuO_4 and $BiNiO_3$. V_2OPO_4 is unique in that the high-temperature phase can be stabilized by a different kind of lattice distortion: V-V dimerization. In the present work, charge/orbital ordered/disordered states in Ca_2RuO_4, $BiNiO_3$ and V_2OPO_4 are analyzed based on mean-field calculations on multiband *d-p* models. Based on the calculated results, the mechanism of NTE of the three systems is discussed.

METHODS

The spin-charge-orbital order/disorder transitions are analyzed by mean-field calculations on *d-p* models in which the *d-d* Coulomb interaction is expressed by Kanamori parameters u, u' and j with $u' = u-2j$[10,11]. The transfer integrals between the transition-metal d and oxygen 2p orbitals are given by Slater-Koster parameters (pds) and (pdp) with the ratio (pdp)/(pds) = -0.45. Following the previous studies on the *d-p* model for 3d and 4d transition-metal oxides[11,12], u' and j are set to 3.0 and 0.5 eV for Ca_2RuO_4, 7.0 and 0.8 eV for $RNiO_3$, and 4.0 and 0.7 eV for V_2OPO_4. (pds) is set to -2.4, -1.8, and -2.0 eV, and charge transfer energy Δ from the oxygen 2p to transition-metal d orbitals is 2.0, 0.0, and 6.0 eV for Ca_2RuO_4, $RNiO_3$, and V_2OPO_4, respectively. The transfer integrals are scaled with the bond length by using Harrison's rule with the exponent of -3.5. The interplay between the orbital ordering and the distortion of the RuO_6 octahedron is studied for Ca_2RuO_4[12]. As for $RNiO_3$, following the mean field calculation on the negative *U* Hubbard model for $BiNiO_3$[13], the previous *d-p* model work for the ground state[14] is extended to the finite temperature. The interplay between the V-V dimer and the orbital order in V_2OPO_4 is examined based on the previous study on $BaV_{10}O_{15}$[15].

RESULTS AND DISCUSSION

Layered perovskite-type Ca_2RuO_4 exhibits an insulator-metal transition around 350 K and an antiferromagnetic transition at 110 K [Figure 1B][16-19]. RuO_6 octahedra share their corners forming a square lattice of Ru in the ab plane of the layered perovskite. The Ru 4d t_{2g} orbitals accommodate four electrons (two holes) in the low spin configuration. In the low (high) temperature phase of Ca_2RuO_4, the RuO_6 octahedron is compressed (elongated) along the c-axis or the z-axis and the *xy* (*yz*/*zx*) orbital is stabilized relative to the *yz*/*zx* (*xy*) orbital among the three t_{2g} orbitals. As shown in Figure 1C, the orbital occupancy change due to the compression and elongation of the octahedron can be described by mean-filed calculations although the spin and orbital fluctuations are not considered. The compressed case has no orbital degrees of freedom. In the elongated case, the doubly degenerate *yz*/*zx* orbitals accommodate one hole per Ru site which may provide orbital entropy of $k_B$log2 and spin entropy of $k_B$log3 in the localized limit of $S = 1$. If the Ru 4d *yz*/*zx* electrons are fully itinerant, the spin and orbital entropy should be reduced. However, the strong electronic correlation in Ca_2RuO_4 suggests that the orbital contribution may remain even in the metallic phase.

The spin entropy can be reduced even in the paramagnetic insulating phase since the space-time fluctuations of spin and orbital are restricted by Ru 4d spin-orbit interaction[3]. While the RuO_6 octahedron is strongly compressed in the antiferromagnetic insulating phase, it is almost regular in the paramagnetic insulating phase. When the energy splitting between the *xy* and *yz*/*zx* orbitals becomes comparable or smaller than the spin-orbit interaction, the three t_{2g} orbitals are mixed to form the complex orbitals of

$$\varphi_1 = \alpha\left(\frac{yz\uparrow - zx\uparrow}{\sqrt{2}}\right) - i\beta\, xy\downarrow \quad (1)$$

and

$$\varphi_2 = \alpha\left(\frac{yz\downarrow + zx\downarrow}{\sqrt{2}}\right) + i\beta\, xy\uparrow \quad (2)$$

where ↑ and ↓ indicate spin up and down. Under the strong spin-orbit interaction, $\alpha = \sqrt{2/3}, \beta = \sqrt{1/3}$. When the two holes occupy these two orbitals in this limit, the spin and orbital entropy can be quenched. The effect of the spin-orbit interaction is weakened in the metallic phase and the spin and orbital fluctuations can revive. Therefore, the metallic phase with elongated octahedron would have substantial electronic entropy higher than that of the paramagnetic insulating phase. The spin and orbital entropy released by the orbital transition may help the NTE discovered in Ca_2RuO_4[4].

Perovskite-type RNiO$_3$ (R = rare earth) becomes insulating at low temperatures due to charge disproportionation of $2Ni^{3+} \rightarrow Ni^{2+} + Ni^{4+}$. The metallic phase has smaller volume and is thus stabilized by pressure, as schematically shown in Figure 2A[20-22]. The charge disproportionation is stabilized by the breathing type distortion of the NiO_6 octahedra, as illustrated in Figure 2B. The effect of the breathing type distortion can be studied by mean-filed calculations on the perovskite-type *d*-*p* model. The results [Figure 2C] indicate that, without the distortion, the various magnetic states with orbital orderings are stable. Even the small breathing type distortion limits the orbital state, and the G-type and C-type antiferromagnetic solutions are excluded. With further increase in the distortion, the compressed site becomes nonmagnetic, and the ferromagnetic and A-type antiferromagnetic solutions degenerate in energy. The O 2p-to Ni 3d charge-transfer energy is almost zero or even negative in RNiO$_3$[23-25]. As a result, the electronic configuration of Ni^{3+} is given by d^8L hybridized with d^7. For simplicity, the Ni^{3+} state with d^8L-d^7 hybridization is described as d^8L in this article. Here, it should be noted that the oxygen hole states represented by L are constructed from the O 2p orbitals in the NiO_6 octahedron and have the same orbital symmetry as the Ni 3d orbitals. Therefore, the d^8L state (hybridized with d^7) cannot avoid the Jahn-Teller instability for the low spin d^7 configuration where one of the doubly degenerate e_g orbitals is occupied by

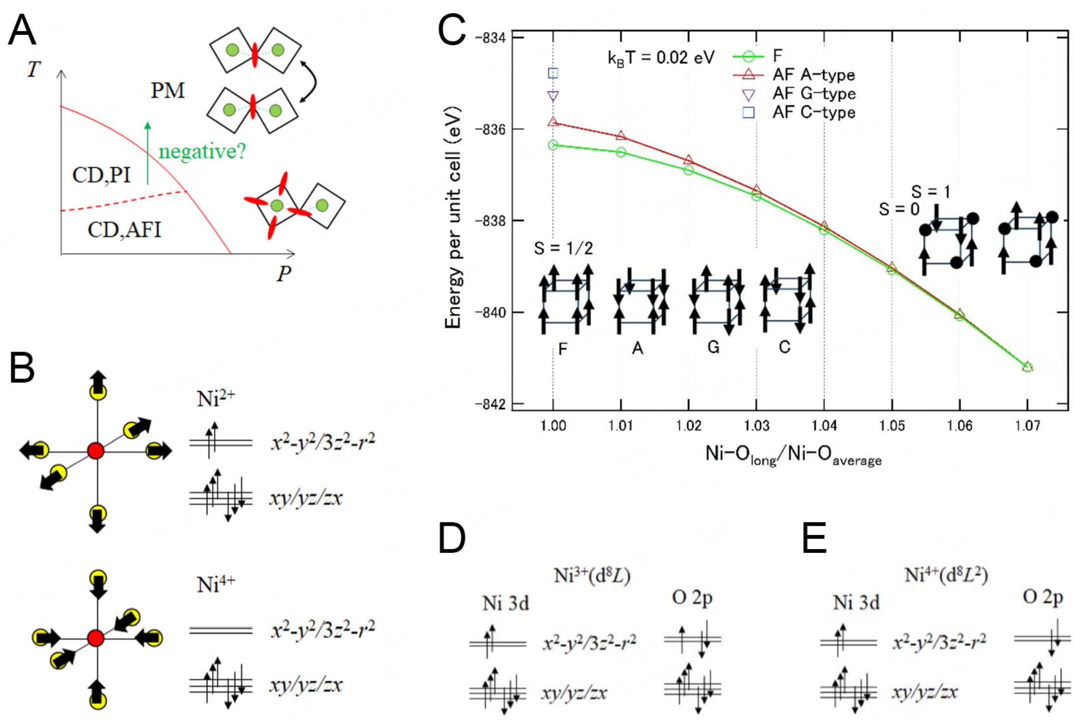

Figure 2. (A) Schematic phase diagram for $RNiO_3$ as functions of temperature T and pressure P. PI, AFI, PM, and CD represent paramagnetic insulating, antiferromagnetic insulating, paramagnetic metallic, and charge disproportionated phases. (B) Distortions of the NiO_6 octahedron and the electronic configurations for the charge disproportionated Ni^{2+} and Ni^{4+} sites without oxygen 2p holes. The yellow and red circles indicate oxygen and transition metal ions, respectively. (C) Energy per unit cell for ferromagnetic and antiferromagnetic (A, G, and C type) states calculated by mean-filed approximation for the perovskite-type *d-p* model with d^7 as a function of breathing distortion (the ratio between the long and average Ni-O bond length). Without the distortion, each site takes the low spin d^7 state with $S = 1/2$. With the distortion, the expanded site becomes d^8 ($S = 1$) and the compressed site becomes d^6 ($S = 0$). (D) Electronic configuration of d^8L. (E) Electronic configuration of d^8L^2.

one electron. In the case of the low spin d^8L state, one of the doubly degenerate L states with e_g symmetry is occupied by one hole [Figure 2D]. The charge disproportionation corresponds to oxygen hole transfer to the Ni^{4+} site where the actual electronic configuration is nonmagnetic d^8L^2 [Figure 2E]. With the charge disproportionated state of d^8 and d^8L^2, the NiO_6 octahedron undergoes breathing distortion rather than Jahn-Teller distortion. The d^8L^2 state (hybridized with d^7L and d^6) of Ni^{4+} is also identified in $SrNiO_3/LaFeO_3$ heterostructure[26].

Since the phase diagram of $RNiO_3$ resembles that of Ca_2RuO_4, $RNiO_3$ itself may exhibit NTE. However, the Ni-O bond length is considerably shortened in the $Ni^{4+}O_6$ octahedron due to the low-spin d^8L^2 configuration which is hybridized with the low-spin d^7L and d^6 configurations. The volume of the charge-disproportionated insulating state is only slightly larger than that of the metallic state, and the NTE effect would be limited. Instead, Azuma *et al.* have established that a sister material $BiNiO_3$ exhibits one of the best NTE performances[6]. In the insulating phase of $BiNiO_3$, the oxygen hole of $Ni^{3+}(d^8L)$ is taken by Bi and the Ni valence becomes +2[18]. As a result, the valence state of $Bi^{3+}{}_{0.5}Bi^{5+}{}_{0.5}Ni^{2+}O_3$ is realized where the configuration of Bi^{5+} is s^2L^2 rather than s^0. Since the Ni^{2+}-O bond length is longer than the Ni^{4+}-O one, the volume of the insulating $BiNiO_3$ is larger than that of the charge disproportionated $RNiO_3$. Also, the Bi $6s^2$ lone pair introduces additional lattice distortions to $BiNiO_3$. As expected, pressure or chemical substitution (such as $Bi_{1-x}La_xNiO_3$) induces a valence transition from $Bi^{3+}{}_{0.5}Bi^{5+}{}_{0.5}Ni^{2+}O_3$ to $Bi^{3+}Ni^{3+}O_3$ with substantial volume collapse[6]. This transition can be viewed as oxygen hole transfer from the Bi^{5+} site to the Ni^{3+} site, and this picture is indeed supported by the recent ab initio calculations[27].

In the NTE $BiNiO_3$, the Ni^{2+}-O-Ni^{2+} superexchange interaction is enhanced due to the relatively small but positive charge-transfer energy (about 4 eV), and the magnetic order (or short-range order) can survive near the Ni-to-Bi charge transfer transition under pressure or with chemical substitution. Therefore, the spin entropy of the insulating $Bi^{3+}_{0.5}Bi^{5+}_{0.5}Ni^{2+}O_3$ tends to be suppressed. The metallic $Bi^{3+}Ni^{3+}O_3$ can be viewed as a charge-disordered metallic state of the charge-disproportionated $R$$NiO_3$. Theoretically, the phase diagram has been studied using mean field calculations on a negative U Hubbard model[13]. In the charge-disordered metallic state, oxygen holes are dissociated from the Ni and Bi sites. Most probably, in the metallic phase of $Bi^{3+}Ni^{3+}O_3$ and $Bi^{3+}_{1-x}La^{3+}_xNi^{3+}O_3$, the d^8L state of Ni^{3+} is disassembled into d^8 at the Ni site and L. While the oxygen hole L is responsible for the metallicity, the localized d^8 state can provide spin entropy of $k_B$log3 per Ni site. This picture is too simplified because the hybridization between the d^8L and d^7 configurations and the band formation are neglected. In the metallic phase, the spin entropy of the localized limit should be reduced due to the d^8L-d^7 hybridization and the band formation. However, substantial spin and charge entropy can remain in the metallic state where the bandwidth is reduced to the order of 0.1 eV by the strong electron-electron and electron-lattice interaction. In this sense, the spin degrees of freedom of Ni $3d^8$ state and the charge degrees of freedom of oxygen hole are correlated in $BiNiO_3$ providing the NTE[6,28].

V_2OPO_4 consists of face-sharing and edge-sharing VO_6 octahedra and is supposed to have a body-centered tetragonal unit cell[7,29]. However, it undergoes V^{2+}/V^{3+} charge ordering at 605 K with monoclinic lattice distortion. The face-sharing V^{2+} and V^{3+} sites form chains along the [110] direction of the monoclinic lattice which corresponds to the a-axis of the tetragonal lattice of the high-temperature phase. The corner-sharing V^{3+} sites are connected approximately along the [001] direction of the monoclinic lattice which is inclined by ~30 degrees relative to the c-axis of the tetragonal lattice. The face-sharing V^{2+} and V^{3+} chain along the [110] direction is illustrated in Figure 3A. The x, y, and z axes are along the V-O bonds. In the present work, a d-p model with a face-sharing octahedron chain is employed. The ferrimagnetic charge-ordered (CO) state is stable only when the V-V bond is elongated or the VO_6 octahedron is elongated along the chain. The spin difference between the neighboring V sites is about 0.6. When the octahedron is close to the regular shape, there is no stable solution. Interestingly, another mean-field solution appears when the V-V bond is substantially compressed. In this solution, the spin difference between the neighboring V sites is as small as 0.1, indicating formation of the molecular orbital (MO) as illustrated in Figure 3B. The calculated energies are plotted as a function of compression/elongation along the V-V bond [Figure 3C].

In the real system, the VO_6 octahedron of V^{3+} is compressed along the z-axis in the CO phase. Therefore, the xy orbital is lower in energy than the yz/zx orbitals. Considering the Hund coupling, one of the yz/zx orbitals is occupied at the V^{3+} site as shown in Figure 3A. Such orbital order is consistent with polarization dependence of V 2p X-ray absorption spectrum[9]; consequently, the orbital fluctuation is quenched. V_2OPO_4 exhibits a ferrimagnetic transition at 165 K. In the ferrimagnetic CO phase, V^{2+} and V^{3+} spins are antiferromagnetically arranged along the face-sharing bond. The antiferromagnetic coupling is consistent with the orbital state in Figure 3A since all the xy, yz, zx electrons are equally transferred to the neighboring site via the V-V and V-O-V pathways in the face-sharing V_2O_9 cluster. Above 165 K, the magnetic susceptibility shows a paramagnetic moment of 1.61 μ_B per V_2OPO_4 unit. The reduction from the ionic values for V^{2+} and V^{3+} spin suggests the effect of spin-orbit interaction or partial singlet bond formation. In the high-temperature phase, the charge order is destroyed and the compression of the $V^{3+}O_6$ octahedron disappears. With the face-sharing geometry, the trigonal ligand field becomes important and the t_{2g} orbitals are split into a_{1g} and e_g^{π} orbitals. In such a situation, the a_{1g} orbitals can form bonding and antibonding

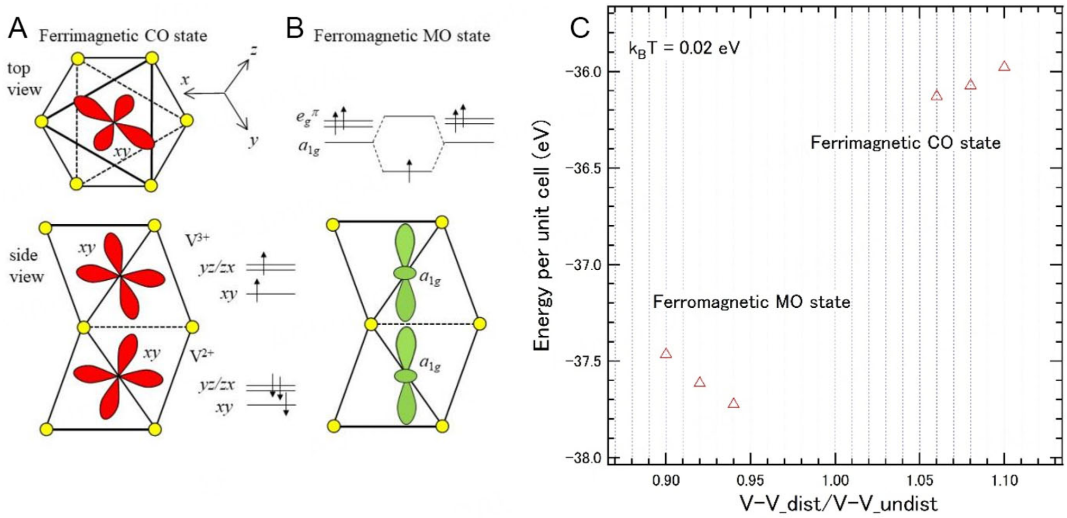

Figure 3. (A) Ferrimagnetic CO state viewed along the face-sharing VO_6 chain and from the side of the chain. The yellow circles indicate oxygen ions. The *x*, *y*, and *z* axes are along the V-O bonds. (B) Ferromagnetic MO state viewed from the side of the chain. The a_{1g} orbitals form the MO. (C) Energy per unit cell (open triangles) calculated by mean-filed approximation for the face-sharing octahedron *d-p* model with $d^{2.5}$ as a function of compression/elongation along the V-V bond (ratio between the compressed/elongated V-V bond length and the original V-V bond length).

orbitals [Figure 3B]. This situation is similar to those of Ti_2O_3[30,31] and $BaV_{10}O_{15}$[15]. Since the bonding orbital is occupied by one electron (two electrons) in the ferromagnetic (ferrimagnetic) state, the V-V bond length is shortened which is consistent with the reduction of the c-axis lattice constant above the transition temperature. On the other hand, the e_g^π electrons remain localized with spin, charge, and orbital fluctuations. In the ferrimagnetic arrangement, the four e_g^π orbitals of the face-sharing V_2O_9 cluster accommodate three electrons providing entropy of $k_B$log4 per cluster. In addition, the spin 1/2 and the spin 1 have $k_B$log2 and $k_B$log3, respectively. Since the tetragonal phase above 605 K with average $V^{2.5+}$ valence has a smaller volume than the monoclinic phase with V^{2+} and V^{3+} charge order, NTE is realized around 605 K, as reported by Pachoud *et al.*[7,29]. The NTE in V_2OPO_4 is driven by the charge transfer between V^{2+} and V^{3+} sites which is coupled with spin and orbital degrees of freedom and the orbital dependent bond formation. The a_{1g}-a_{1g} bonds keep the smaller volume while the spin, charge, and orbital fluctuations of the e_g^π electrons provide entropy higher than the charge/orbital ordered phase.

CONCLUSIONS

Based on the mean-field calculations on the *d-p* models, the relationship between the charge/orbital states and the lattice distortion has been discussed for Ca_2RuO_4, RNiO$_3$, and V_2OPO_4. The changes of the charge/orbital states by the lattice distortion suggest their disordered states harbor relatively high entropy due to charge/orbital fluctuations. Across the insulator-metal transition in Ca_2RuO_4, the RuO_6 octahedron is elongated and the *yz*/*zx* orbital fluctuation becomes relevant in the metallic phase. The *yz*/*zx* orbital fluctuation in the metallic phase is intimately related to the orbital-dependent band renormalization in the metallic phase of $Ca_{2-x}Sr_xRuO_4$[32]. Above the transition temperature of Ca_2RuO_4, the strongly renormalized Ru 4d electrons (bandwidth ~0.1 eV) are almost incoherent and exhibit localized character. The insulator-metal transition in $BiNiO_3$ is accompanied by the oxygen hole transfer from Bi to Ni. In V_2OPO_4, the charge/orbital disordered state has relatively small volume due to the a_{1g}-a_{1g} bond in the face-sharing octahedra while the spin, charge, and orbital fluctuations of the e_g^π electrons provide higher entropy than the charge/orbital ordered state. In Ca_2RuO_4 and V_2OPO_4, the orbital-dependent fluctuations of the t_{2g} electrons play key roles in realizing the NTE behaviors. While the orbital order/disorder is coupled with the

Jahn-Teller distortion in the corner-sharing octahedra of Ca_2RuO_4, it is governed by the metal-metal dimerization in the face-sharing octahedra of V_2OPO_4. Such t_{2g} electron systems with orbital ordering can be candidates for new NTE materials. Orbital and/or charge states are rearranged across their insulator-metal transitions of Ca_2RuO_4 and $BiNiO_3$, and the metallic phases with orbital and/or charge fluctuations can be stabilized at high temperatures relative to the insulating phases without them. The negative charge-transfer energy and the oxygen 2p holes are responsible for the charge-transfer mechanism and provide the charge fluctuations in the high-temperature phase of $BiNiO_3$. In Ca_2RuO_4, the Jahn-Teller distortion gradually develops below the transition temperature due to the spin-orbit coupling[3]. The spin-orbit interaction would be important in the extremely wide temperature range of NTE in Ca_2RuO_4.

DECLARATIONS

Acknowledgments

The author would like to thank Prof. G. A. Sawatzky, Prof. L. H. Tjeng, Prof. S. Nakatsuji, Prof. Y. Maeno, Prof. D. I. Khomskii, Prof. M. Azuma, Prof. J. P. Attfield, and the members of their research groups for long-term collaborations on the target materials of this article.

Authors' contributions

The author contributed solely to the article.

Availability of data and materials

Data supporting the findings of this article are available from the author upon reasonable request.

Financial support and sponsorship

This work was supported by the JSPS KAKENHI Grant (No. JP22H01172).

Conflicts of interest

The author declared that there are no conflicts of interest.

Ethical approval and consent to participate

Not applicable.

Consent for publication

Not applicable.

REFERENCES

1. Imada, M.; Fujimori, A.; Tokura, Y. Metal-insulator transitions. *Rev. Mod. Phys.* **1998**, *70*, 1039-263. DOI
2. Khomskii, D. I. Transition metal compounds. Cambridge University Press; 2014. DOI
3. Mizokawa, T.; Tjeng, L. H.; Sawatzky, G. A.; et al. Spin-orbit coupling in the Mott insulator Ca_2RuO_4. *Phys. Rev. Lett.* **2001**, *87*, 077202. DOI
4. Takenaka, K.; Inoue, N.; Mizuno, Y.; et al. Extended operating temperature window of giant negative thermal expansion in Sn-doped Ca_2RuO_4. *Appl. Phys. Lett.* **2018**, *113*, 071902. DOI
5. Alonso, J. A.; García-Muñoz, J. L.; Fernández-Díaz, M. T.; Aranda, M. A. G.; Martínez-Lope, M. J.; Casais, M. T. Charge disproportionation in $RNiO_3$ perovskites: simultaneous metal-insulator and structural transition in $YNiO_3$. *Phys. Rev. Lett.* **1999**, *82*, 3871-4. DOI
6. Azuma, M.; Chen, W. T.; Seki, H.; et al. Colossal negative thermal expansion in $BiNiO_3$ induced by intermetallic charge transfer. *Nat. Commun.* **2011**, *2*, 347. DOI PubMed PMC
7. Pachoud, E.; Cumby, J.; Lithgow, C. T.; Attfield, J. P. Charge order and negative thermal expansion in V_2OPO_4. *J. Am. Chem. Soc.*

2018, *140*, 636-41. DOI PubMed

8. Murota, K.; Pachoud, E.; Attfield, J. P.; et al. Charge correlation in V_2OPO_4 probed by hard x-ray photoemission spectroscopy. *Phys. Rev. B.* **2020**, *101*, 235159. DOI
9. Murota, K.; Pachoud, E.; Attfield, J. P.; et al. Vanadium 3d charge and orbital states in V_2OPO_4 probed by x-ray absorption spectroscopy. *Phys. Rev. B.* **2020**, *101*, 245106. DOI
10. Mizokawa, T.; Fujimori, A. Unrestricted hartree-fock study of transition-metal oxides: spin and orbital ordering in perovskite-type lattice. *Phys. Rev. B. Condens. Matter.* **1995**, *51*, 12880-3. DOI PubMed
11. Mizokawa, T.; Fujimori, A. Electronic structure and orbital ordering in perovskite-type 3d transition-metal oxides studied by Hartree-Fock band-structure calculations. *Phys. Rev. B. Condens. Matter.* **1996**, *54*, 5368-80. DOI PubMed
12. Kurokawa, M.; Mizokawa, T. Orbital state and metal-insulator transition in $Ca_{2-x}Sr_xRuO_4$ studied by model Hartree-Fock calculations. *Phys. Rev. B.* **2002**, *66*, 024434. DOI
13. Naka, M.; Seo, H.; Motome, Y. Theory of valence transition in $BiNiO_3$. *Phys. Rev. Lett.* **2016**, *116*, 056402. DOI
14. Mizokawa, T.; Khomskii, D. I.; Sawatzky, G. A. Spin and charge ordering in self-doped Mott insulators. *Phys. Rev. B.* **2000**, *61*, 11263-6. DOI
15. Yoshino, T.; Okawa, M.; Kajita, T.; et al. Unusual valence state and metal-insulator transition in $BaV_{10}O_{15}$ probed by hard x-ray photoemission spectroscopy. *Phys. Rev. B.* **2017**, *95*, 075151. DOI
16. Mizokawa, T.; Tjeng, L. H.; Lin, H.; et al. Orbital state and metal-insulator transition in $Ca_{2-x}Sr_xRuO_4$ (x=0.0 and 0.09) studied by x-ray absorption spectroscopy. *Phys. Rev. B.* **2004**, *69*, 132410. DOI
17. Nakamura, F.; Goko, T.; Ito, M.; et al. From mott insulator to ferromagnetic metal: a pressure study of Ca_2RuO_4. *Phys. Rev. B.* **2002**, *65*, 220402. DOI
18. Steffens, P.; Friedt, O.; Alireza, P.; et al. High-pressure diffraction studies on Ca_2RuO_4. *Phys. Rev. B.* **2005**, *72*, 094104. DOI
19. Keen, H. D. J.; Julian, S. R.; Hermann, A. *Ab initio* study of pressure-induced structural and electronic phase transitions in Ca_2RuO_4. *Phys. Rev. B.* **2021**, *104*, 085143. DOI
20. Torrance, J. B.; Lacorre, P.; Nazzal, A. I.; Ansaldo, E. J.; Niedermayer, C. Systematic study of insulator-metal transitions in perovskites $RNiO_3$ (R=Pr,Nd,Sm,Eu) due to closing of charge-transfer gap. *Phys. Rev. B. Condens. Matter.* **1992**, *45*, 8209-12. DOI
21. Zhou, J. S.; Goodenough, J. B.; Dabrowski, B. Pressure-induced non-Fermi-liquid behavior of $PrNiO_3$. *Phys. Rev. Lett.* **2005**, *94*, 226602. DOI PubMed
22. Cheng, J.; Zhou, J.; Goodenough, J. B.; Alonso, J. A.; Martinez-lope, M. J. Pressure dependence of metal-insulator transition in perovskites $RNiO_3$ (R=Eu , Y, Lu). *Phys. Rev. B.* **2010**, *82*, 085107. DOI
23. Mizokawa, T.; Fujimori, A.; Arima, T.; Tokura, Y.; Mori, N.; Akimitsu, J. Electronic structure of $PrNiO_3$ studied by photoemission and x-ray-absorption spectroscopy: band gap and orbital ordering. *Phys. Rev. B. Condens. Matter.* **1995**, *52*, 13865-73. DOI PubMed
24. Johnston, S.; Mukherjee, A.; Elfimov, I.; Berciu, M.; Sawatzky, G. A. Charge disproportionation without charge transfer in the rare-earth-element nickelates as a possible mechanism for the metal-insulator transition. *Phys. Rev. Lett.* **2014**, *112*, 106404. DOI PubMed
25. Green, R. J.; Haverkort, M. W.; Sawatzky, G. A. Bond disproportionation and dynamical charge fluctuations in the perovskite rare-earth nickelates. *Phys. Rev. B.* **2016**, 94. DOI
26. Wang, L.; Yang, Z.; Bowden, M. E.; et al. Hole-trapping-induced stabilization of Ni^{4+} in $SrNiO_3/LaFeO_3$ superlattices. *Adv. Mater.* **2020**, *32*, e2005003. DOI
27. Paul, A.; Mukherjee, A.; Dasgupta, I.; Paramekanti, A.; Saha-Dasgupta, T. Hybridization-switching induced mott transition in ABO_3 perovskites. *Phys. Rev. Lett.* **2019**, *122*, 016404. DOI
28. Nishikubo, T.; Sakai, Y.; Oka, K.; et al. Optimized negative thermal expansion induced by gradual intermetallic charge transfer in $Bi_{1-x}Sb_xNiO_3$. *Appl. Phys. Express.* **2018**, *11*, 061102. DOI
29. Pachoud, E.; Cumby, J.; Wright, J.; Raguz, B.; Glaum, R.; Attfield, J. P. Electronic origin of negative thermal expansion in V_2OPO_4. *Chem. Commun.* **2020**, *56*, 6523-6. DOI PubMed
30. Chang, C.; Koethe, T.; Hu, Z.; et al. c-axis dimer and its electronic breakup: the insulator-to-metal transition in Ti_2O_3. *Phys. Rev. X.* **2018**, *8*, 021004. DOI
31. Miyoshino, T.; Takegami, D.; Meléndez-Sans, A.; et al. Intra c-axis dimer hybridization and mixed valency in Mg-doped Ti_2O_3. *Phys. Rev. B.* **2023**, *107*, 115145. DOI
32. Kim, M.; Kwon, J.; Kim, C. H.; et al. Signature of Kondo hybridisation with an orbital-selective Mott phase in 4d $Ca_{2-x}Sr_xRuO_4$. *NPJ. Quantum. Mater.* **2022**, *7*, 471. DOI